CDF Top Quark Mass Measurement with the Matrix Element Method
Report
Summer Students at Fermi National Accelerator Laboratory

Gabriele Franciolini
Supervisor: Prof. George Velev

Dipartimento di Fisica "E. Fermi" - Università di Pisa
Fermi National Accelerator Laboratory

Abstract

This report describes the contribution of the author to the measurement of the Top mass using the matrix element method on the RunII data sample in collaboration with the CDF research group. Part of my work focused on testing the new quasi-MC integration code for the signal. The second part dealt with testing the new transfer functions. The final part involved the preliminary analysis of the dependence of the results for M_t and Δ_{JES} to the $\Delta_{JES,MC}$ of the montecarlo's simulated events.

Fermilab

Period: 07-25-2016 / 09-23-2016

Contents

1 Introduction

1.1 Top quark and SM parameters

The quark top is one of the fundamental particles of the SM. It was discovered in 1995 at the Tevatron collider at Fermilab during the Run I by the CDF and $D\emptyset$ experiments. This discovery was one of the key steps for the validation of the quark model for hadrons and the standard model itself. The quark top is a fermion with spin =1/2 and electromagnetic charge = $+2/3\,|e|$; it carries color charge and has a mass of $m_t \sim 173 GeV/c^2$. The quark top interacts through all the known fundamental forces: gravitational, electromagnetic, weak and strong force. The only parameter that was not predicted by the theory is its mass, which has been studied since the discovery and its best determination is one of the goal of the CDF collaboration.

In the experiment conducted at Tevatron collider, top quarks are produced mainly from strong processes: $q\bar{q} \to t\bar{t}$ (85% at Tevatron energies) and $g\bar{g} \to t\bar{t}$. At energies of $\sqrt{s} = 1.96 TeV$ those production cross sections can be calculated with perturbative QCD and are found in agreement with the measured value of [10]:

$$\sigma_{t\bar{t}} = 7.16^{+0.11+0.17}_{-0.20-0.12}\ pb. \tag{1.1}$$

The other important property of the top quark it is its decay channels. The top quark can decay in a down-type quark (d,s,b) and its decay rates are proportional to the squared CKM matrix element. The value of $|V_{tb}|^2$ has been measured [3]:

$$|V_{tb}|^2 = 1.02^{+0.29}_{-0.31}. \tag{1.2}$$

Given that value and the unitarity of the CKM matrix, the fraction of the quark top branching ratio of decay in b-quark and all down-type quark is:

$$R = \frac{B(t \to Wb)}{B(t \to Wq)} = \frac{|V_{tb}|^2}{|V_{td}|^2 + |V_{ts}|^2 + |V_{tb}|^2} \sim 1 \tag{1.3}$$

making the b decay channel probability of almost 100%. The top decay width Γ_t is of order of magnitude of $\sim 1 GeV$, which is larger that the typical QCD scale of $200 MeV$. For that reason the lifetime is much smaller than the typical time of formation of QCD bound state hadrons (top-flavoured hadrons or $t\bar{t}$-quarkonium), so the top quark decays before those states can be formed.

1.2 Top mass Measurements

As stated before, the mass of the quark top is the only parameter which is not predicted by the SM. Therefore having a good measurement of his mass it is very important. It has effects on the precisions of the predictions of the SM. The last world combination of measurement of the Top quark mass has been performed in 2014 with the latest measurements available at that time from Tevatron (CDF, $D\emptyset$) and LHC (ATLAS, CMS). In image 1.1 all the different measurements are reported. The result is [2]:

$$M_t = 173.34 \pm 0.27_{stat} \pm 0.71_{syst} GeV/c^2 \tag{1.4}$$

reaching a precision of 0.44%.

The latest single measurement from both the labs reached an higher precision. In fact the most recent $D\emptyset$ measurement is [4]:

$$M_t = 174.98 \pm 0.58_{stat+JES} \pm 0.49_{syst} GeV/c^2 \tag{1.5}$$

with a precision of 0.43%. This measurement was carried out with the matrix element method. The most precise result was found by the last CMS measurement [6]:

$$M_t = 172.44 \pm 0.13_{stat} \pm 0.44_{syst} GeV/c^2 \tag{1.6}$$

reaching a precision of 0.28%. In this context, the aim of the CDF collaboration is twofold. Firstly, the goal is to reach the highest possible precision exploiting the full RunII data collected by CDF between 2001 and 2011. Furthermore, it is interesting to examine the tension between LHC (1.6) and Tevatron (1.5) measurement which have a separation greater than 3σ. CDF has already completed a first measurement of the quark top mass using the matrix element method that is implemented in this analysis but with only part of the RunII dataset. This [5] result is taken as reference for our analysis:

$$M_t = 173.0 \pm 1.2 GeV/c^2 \tag{1.7}$$

In the following sections there is the description of all the improvements scheduled to be implemented in this analysis compared to the old one.

1.3 Channel selection and ME method

In order to measure the mass of the top we are interested in events which creates $t\bar{t}$ couples. Those events can be selected depending on their signature. The decay signature can be classified as follows:

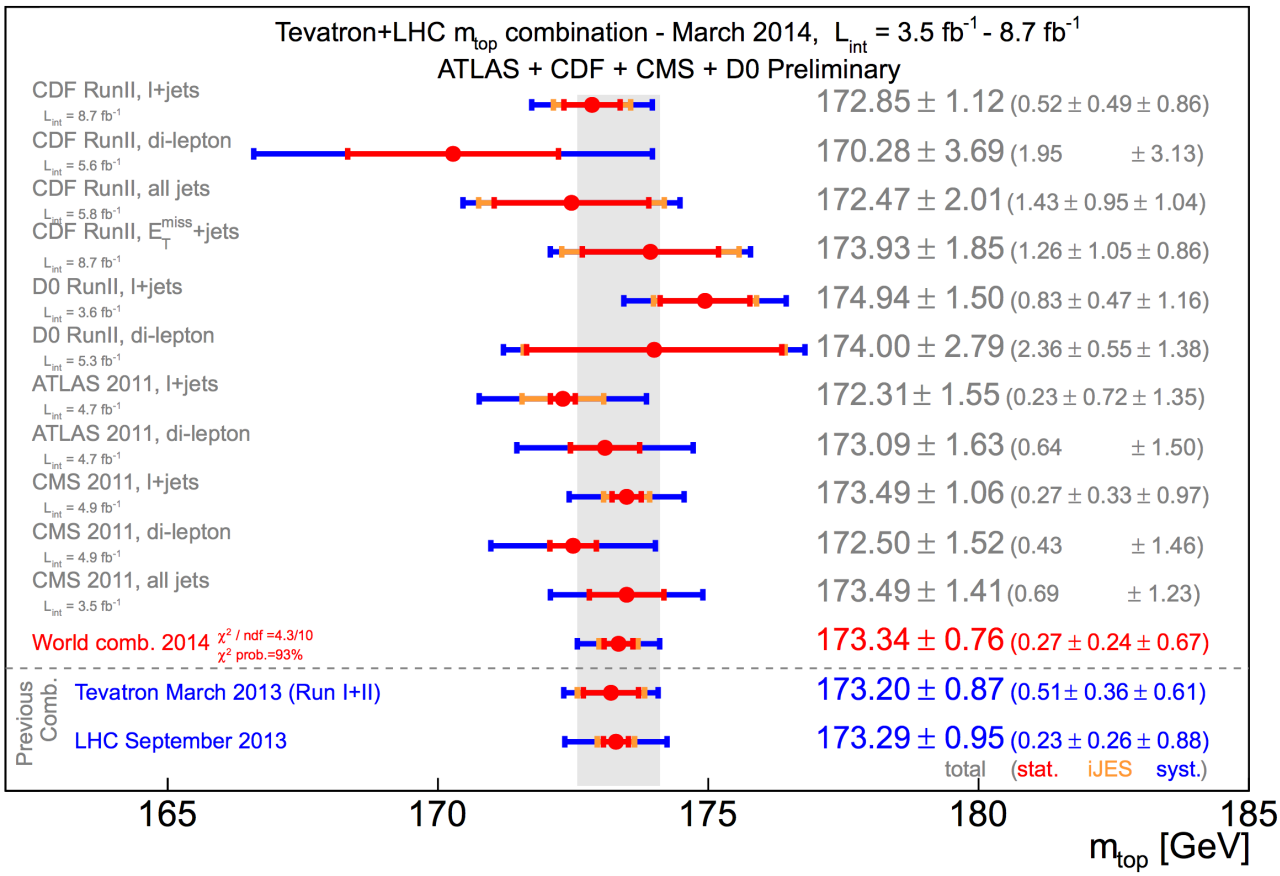

Figure 1.1: Latest world combination performed in 2014 with results from Tevatron and LHC.

– *Dilepton events*: $t\bar{t} \rightarrow [l, \nu_l + l', \nu_{l'} + jets]$ where both W decay into the leptonic channel. It has the cleanest signature and highest signal-to-background ratio but occurs only in $\sim 7\%$ of cases and by having 2 undetected ν_l it has an unconstrained kinematics;

– *Hadronic events*: $t\bar{t} \rightarrow [hadrons]$ where both W decay hadronically (at least 6 jets). It has $\sim 55\%$ of decay rate but it presents a large QCD background;

– *Lepton+Jets events*: $t\bar{t} \rightarrow [l, \nu_l + jets]$ where one W decays leptonically and the other W decays hadronically. It accounts for $\sim 38\%$ of the decays while providing a distinct experimental signature through the isolated lepton and a good signal-to-background ratio. For that reason this is the optimal channel for our measurement.

The event signature that we require for the *lepton+jets* events is: charged lepton with high p_t, large missing transverse energy $\not\!\!E_t$ and at least 4 jets. Those events can be divided in different categories. We define a *tight* jet as a jet with $E_t > 20GeV$ and $|\eta| \leq 2.0$ and a *loose* jet one having $E_t > 12GeV$ and $|\eta| \leq 2.4$. A tight event is then an event with exactly 4 thigh jets while we define the rest as loose events. Finally we defined a tagged jet if the jet is identified as resulting from the hadronization of a b quark coming from the W decay. In this analysis the following categories are considered: 0Tag, 1TagT, 1TagL, 2TagT, 2TagL (the T and L stands for tight and loose respectively). In Figure 1.2 there are all the categories' selection requirements.

The possible events not coming from $t\bar{t}$ decay that can mimic the lepton+jets signature can be divide as follows:

– W+jets: events with W decaying into leptonic channel and a number of hadronic jets. This is the most important background source;

– QCD: multi-jet events which leave a leptonic signature by "fake electron" (jets misidentified as electrons in the electromagnetic calorimeter) or secondary electrons (coming from lep-

	0-tag	1-tagT	1-tagL	2-tagT	2-tagL
Lepton E_T [GeV]	> 20	> 20	> 20	> 20	> 20
Lepton $\|\eta\|$	$0-1$	$0-1$	$0-1$	$0-1$	$0-1$
$\not\!\!E_T$ [GeV]	20	20	20	20	20
Leading 3 jets E_T [GeV]	20	20	20	20	20
Leading 3 jets η	$0-2$	$0-2$	$0-2$	$0-2$	$0-2$
4^{th} jet E_T [GeV]	> 20	> 20	> 12	> 20	> 12
4^{th} jet η	$0-2$	$0-2$	$0-2.4$	$0-2$	$0-2.4$
Extra jets E_T [GeV]	< 20	Any loose	Any loose or ≥ 1 tight	Any loose	Any loose or ≥ 1 tight

Figure 1.2: Selection requirements depending on the number of b-tag and tight and loose jets

tonic decays inside jets);

- Single top: a W and b coming from top decay with other jets. It has a relative smaller contribution;
- Diboson: WW,WZ,ZZ events that can create the lepton+jets signature;
- Z+jets: as W+jets can generate a semileptonic event signal.

The Matrix Element method is the optimal method to measure parameters of the SM, provided that one have a very robust theoretical model and detector response model. The measurement is performed on candidate $t\bar{t}$ events in the channel and categories already defined. For every event the probability of observing that event is computed by integrating the matrix element for $t\bar{t}$ production and decay over the 32 dimensional phase space variables (actually reduced to 19 with constraint and assumptions). The likelihood for a signal event is defined as [5]:

$$L_{sgn}(\vec{y}|M_t,\Delta_{JES}) = \frac{1}{N(M_t)}\frac{1}{A(M_t,\Delta_{JES})}\sum_{i=1}^{24} w_i \left[\int \frac{f(z_1)f(z_2)}{FF} TF(\vec{y}|\vec{x},\Delta_{JES})|M(M_t,\vec{x})|^2 d\Phi(\vec{x})\right]_i \quad (1.8)$$

where $\vec{y}$ are the quantities measured in the detector, $\vec{x}$ are the parton-level quantities that defines the kinematics of the event, $N(M_t)$ is the global normalisation factor (including $\sigma_{p\bar{p}\to t\bar{t}}$), $A(M_t,\Delta_{JES})$ is the acceptance, $f(z_1)$ and $f(z_2)$ are the PDFs for incoming parton momentum fraction z_j, FF is the relativistic flux factor, $TF(\vec{y}|\vec{x},\Delta_{JES})$ are the transfer functions. $M(M_t,\vec{x})$ is the Kleiss-Stirling matrix element [8] for both $q\bar{q}\to t\bar{t}$ and $g\bar{g}\to t\bar{t}$ production processes. Because the main source of systematic uncertainty is the jet energy uncertainty, the likelihood is built as a two dimensional function of M_t and Δ_{JES}. The Δ_{JES} is a correction factor which correct jet energies by a factor of $1+\Delta_{JES}\sigma_j$, where σ_j is the fractional systematic uncertainty on the energy for a given jet. To have a better modelling and reduce the systematic uncertainties, a likelihood for the main background contribution (W+jets) is included in the analysis. A background event from a channel not included in the likelihood will lead to a shift in M_t. Thus the other background channels are going to be taken into account with the final calibration of the method by means of pseudo-experiment.

The two likelihood are combined to form the total likelihood:

$$L_{ev}(\mathbf{y}|m_t,\Delta_{JES}) = a(f_{sig})L_{sig}(\mathbf{y}|m_t,\Delta_{JES}) + b(f_{bkg})L_{bkg}(\mathbf{y}|\Delta_{JES}) \quad (1.9)$$

Once the full definition of the likelihood is implemented in the ME code, several pseudo-experiment are going to be performed in order to tune the combination factors[1]. Finally the results for every event in the data are combined:

$$L(M_t, \Delta_{JES}) = \prod^{events} L_{ev}(\mathbf{y}|m_t, \Delta_{JES}). \quad (1.10)$$

The procedure to extract the value of the M_t is the profiled likelihood method explained in section 4. At this point of the analysis the normalisation and the acceptance are still not included in the ME code. Thus the results of the integration are not proper probabilities and are going to be called weights of integration $W_{k,ij}$, where i, j are the indices forΔ_{JES} and M_t respectively; k is a label that identify the event in the MC samples.

The aim of this measurement is to find the most precise value for the M_t with the full dataset of the Run II of Tevatron. The improvement with respect to the last measurement can be summarised in the following points:

- Increase of the integrated luminosity: from $5.6fb^{-1}$ to $9.0fb^{-1}$;
- Inclusion of the new sample categories: 0TagT, 1TagL, 2TagL;
- Modelling of the background in the matrix element method by the inclusion of the background likelihood term;
- Refinement of the q-MC integration method for a faster event probability computation;
- Usage of NLO signal MC samples for a reduction of systematic uncertainty in the calibration procedure.

2 Integration methods analysis

In this section I present the preliminary work I did to validate the integration method used in the ME code. The Matrix element method heavily rely on the condition of having a fast integration code. As explained in the preceding section section, in order to calculate the probability of a single event, several integrations has to be performed. The integration is stopped if one of the following requirements is satisfied:

- Maximum number of integration points (2^{18});
- Maximum time allowed (7200 s);
- Maximum precision required (0.1).

In brackets are reported the values of the variables used in the code. The aim of the analysis at this point is to improve the MC integration code to have a faster convergence and, consequently, a faster reach of the precision termination condition. Under this perspective having faster converging integration is the key to be able to reach the desired precision in the determination of the likelihood with a restrained computational time.

2.1 p-MC: pull distribution

The first step was to analyse the error estimation for the pseudo MonteCarlo integration code which is the most reliable and robust integration method. The p-MC integration is based on sampling the function in randomly chosen points. The integral of a function defined on a domain $\mathcal{D}$ of dimension d is estimated then as:

$$I = \int_{\mathcal{D}} f(\vec{x})d\vec{x} \approx \frac{1}{N}\sum_{i=1}^{N} f(\vec{x_i}) \quad (2.1)$$

where $\vec{x_i} \sim U[\mathcal{D}]$ and N is the number of points of integration. By the central limit theorem we expect the relative error of integration to be:

$$\frac{\Delta I}{I} = \mathcal{O}(N^{-1/2}) \quad (2.2)$$

independently of the dimension d of the of the integral. This method is combined with the importance sampling, a mathematical trick which allows us to practically modify the distribution of random points to select more points in regions where the function is more important without loosing the MC integration properties. It is achieved by introducing a well behaved density function $g(\vec{x})$ in the integral:

$$I = \int_{\mathcal{D}} f(\vec{x})d\vec{x} = \int_{\mathcal{D}} f(\vec{x})\frac{g(\vec{x})}{g(\vec{x})}d\vec{x}. \quad (2.3)$$

This gives the integral estimation defined as:

$$I \approx \frac{1}{N}\sum_{i=1}^{N}\left(\frac{f(\vec{y_i})}{g(\vec{y_i})}\right) \quad (2.4)$$

where the points are now distributed as: $\vec{y_i} \sim g(\vec{x})$. In order to test the code we run a simulation to build

[1] For perfectly normalised likelihood, they should be $a(f_{sig} = f)$ and $b(f_{bkg}) = 1 - f$.

the pull distribution. Furthermore this pull distribution will be used as comparison in the testing of the new code with the quasi-MC. As input file a sample of MC simulated events has been taken and converted in a format compatible with ME integration code. The sample (A.1) contains 956 LO signal events built with Pythia and the properties shown in table 2.1:

MC sample properties	
$M_{t,MC}$	$173 GeV/c^2$
$\Delta_{JES,MC}$	0σ
category	1TagT

Table 2.1: MC signal events construction properties.

The following procedure has been used to build the pull distribution. For every event, 22 integration have been calculated on the cluster Fermigrid with different random seed for the generation of random points. The mean over the repeated integrations is defined as:

$$< W_{k,ij} >= \frac{1}{22}\sum_{l=1}^{22} W_{k,ij,l}, \tag{2.5}$$

where k label the event ($\in [1, 956]$); i, j label values of $\Delta_{JES}, M_t \in \{[-3, +3]\sigma, [157.5, 187.5] GeV/c^2\}$) of the output; l labels the different integration of the event; $W_{k,ij}$ is the result of the integration as defined in section 1.3. The standard deviation is defined as follows:

$$\sigma_{k,ij} = \sqrt{\frac{1}{21}\sum_{l=1}^{22}(W_{k,ij,l} - < W_{k,ij} >)^2}. \tag{2.6}$$

The pull variable is then the normalised variable:

$$\delta_{k,ij,l} = \frac{W_{k,ij,l} - < W_{k,ij} >}{\sigma_{k,ij}}. \tag{2.7}$$

The Plot 2.1 shows the histogram of the pull variable $\delta_{k,ij,l}$ $\forall(k, i, j, l)$. In the hypothesis that the integration code doesn't have any bias, we expect the pull variable to be distributed as a $N(0, 1)$ and the total histogram to be as close as possible to that distribution.

We can clearly see the presence of a spike in the histogram around ~ 0.2. Before analysing the plot, effort has been put to find the source of this unexpected spike. Two problematic results where identified. In fact events number 58 and 330 where

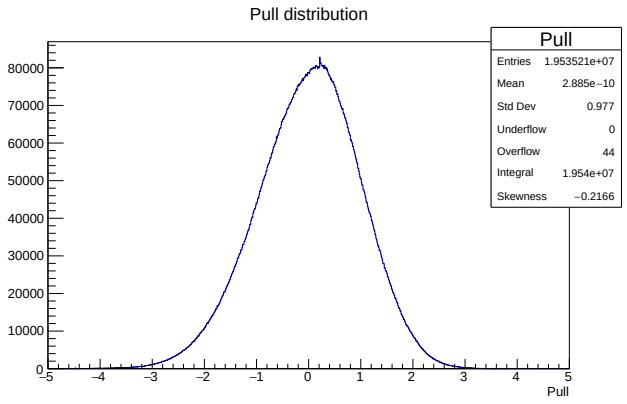

Figure 2.1: Pull histogram for p-MC integration method. It present a unexpected spike which revealed a problem in the pull calculation.

giving numerical problems in the determination of the pull. Since the same complication was found in the q-MC results too, the explanation of the problem and its solution can be found in section 2.2. Thus, by removing the problematic results, the pull for p-MC is obtained (figure 2.2).

It is evident how the pull distribution is very close to a $N(0, 1)$ with the histogram parameters mean and standard deviation being:

$$\mu_{p-MC} = (3.1020 \pm 0.0002) \cdot 10^{-10}; \tag{2.8}$$
$$\sigma_{p-MC} = 0.9770 \pm 0.0001. \tag{2.9}$$

This is a confirmation that the integration code is well implemented and gives consistent results. Still there is a negative skewness which could be the result of some bias in the code. It is not clear if this will go away with more statistics (more than 22 repetition of the integration). More results are needed to have definitive responses.

This is a fundamental result at this stage of the analysis because it give us the opportunity to compare it with the same pull distribution obtained the q-MC method.

2.2 q-MC: pull distribution

The goal of this analysis is to test the new implementation of the q-MC method of integration. The quasi-MC method is very similar to the psedo-MC method of integration with the only difference being in the sequence of points used to evaluate the function and compute the mean value which estimate the integral.

As already stated in the previous section p-MC uses a complete random sequence of points where

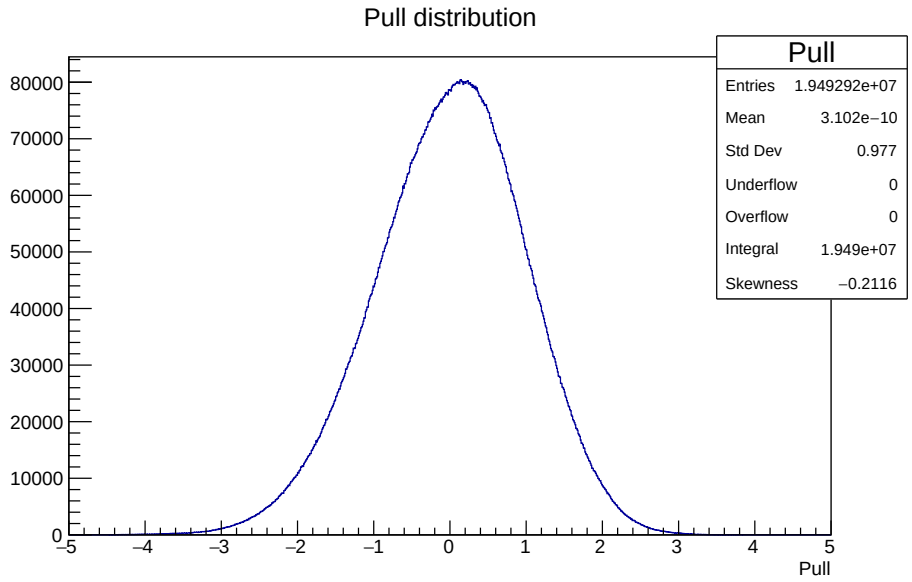

Figure 2.2: Pull histogram for p-MC integration method without results of events 58 and 330.

every $\vec{x_i}$ is independent and identical distributed to the other. In the q-MC instead it is used a deterministic sequence with particular properties. If we define the star discrepancy D^* of a sequence of points P_N in $\mathbb{R}^d$ as:

$$D_N^*(P_N) = Sup_{B\in\mathcal{A}} \left| \frac{\#\{P_N \in B\}}{N} - \lambda(B) \right| \quad (2.10)$$

$$\mathcal{A} = \{\vec{x} \in \mathbb{R}^d : x_i \in [0, b_i) \ \forall 0 < b_i < 1\} \quad (2.11)$$

where $\lambda(B)$ is the Lebesque measure of B. It has been proven that [9]:

$$\left| \frac{1}{N} \sum_{i=1}^{N} f(\vec{x}_i) - \int_{[0,1]^s} f(u)du \right| \leq V(f) D_N^*(\vec{x}_1, ..., \vec{x}_n) \quad (2.12)$$

where $\vec{x}_i$ are points of the sequence P_N and under the hypothesis that the variation of the function $V(f)$ is bounded. This is called the Koksma-Hlawka inequality. So, by using the so called "low discrepancy sequences" it is possible to achieve a better convergence of the relative error of the integral.

The Sobol sequence is a well known low discrepancy sequence. It has been proven that it should give a error convergence of:

$$\frac{\Delta I}{I} = \mathcal{O}(N^{-1+\varepsilon}) \quad (2.13)$$

where ε depends on the properties of the integrand functions as expected.

On top of that, a further scrambling of the points of the sequence has been implemented in the code. There are several random scrambling defined in order to preserve the low discrepancy property but avoiding intrinsic biases of the method and even improve the convergence [7]. Two scrambling methods are implemented in the code: one proposed by Owen and one proposed by Faure and Tezuka. Both of them act as a random scrambling of the point of the sobol sequence without spoiling the LDS property. Even though different points of a certain sequence are not iid, this scrambling ensure us that, with a different random seed for every different integration, the points between two different sequences are iid. So the pull analysis can be performed for the q-MC in the same way as for the p-MC and the results can be compared.

In order to build the pull distribution the same set of events used in the analysis in section 2.1 has been integrated 22 times with different randomised sobol sequences (in the code: sequence "fortsobol", option 3 which sets Owen + Faure-Tezuka scrambling). The pull is again defined with the definitions (2.5), (2.6), (2.7). In plot 2.3 there is the pull distribution. Again the detail that needed to be understood is the presence of that spike at 0.2 which is completely unexpected and shows the presence of some bias in the pull calculation or in the matrix element integration code. In order to find the source of the spike I tried to calculate the pull without some of the 22 output files to see if it was the consequence of some problem in the submission of some particular job on Fermigrid. I didn't find any problem related with an entire job submission of the

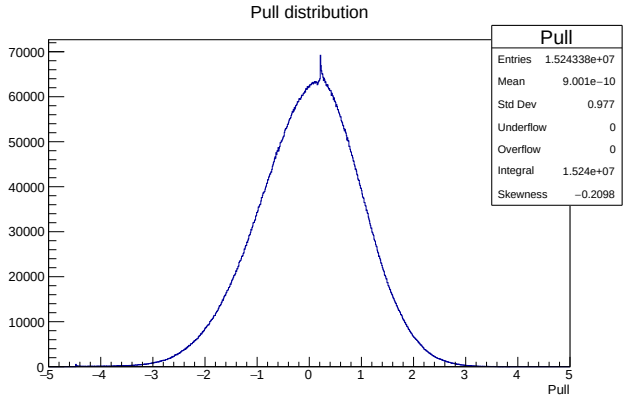

Figure 2.3: Pull histogram for q-MC integration method. The same spike seen in p-MC result is present.

integration. Then I tried to search for some events with a particular kinematics which could lead to extreme results and so introduce some numerical errors in the pull calculation. I found that there were 2 special events that where triggering the spike. In particular event number 58 (figure 2.4) and event 330 (figure 2.5).

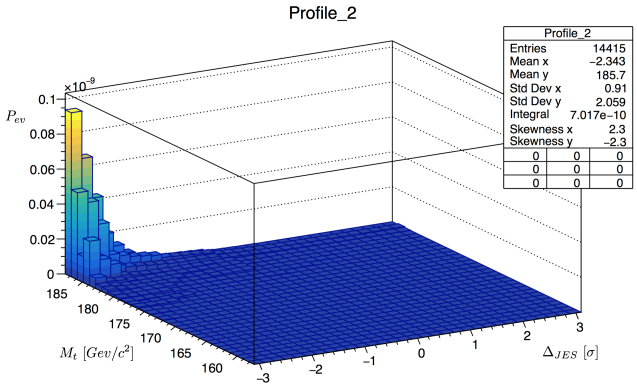

Figure 2.4: Plot of $W_{ij,ev=58}(\Delta_{JES}, M_t)$

In both cases we can clearly see that the majority of the bins have a value of the weight of the integration very close to 0 if not exactly 0. That could be the source of some numerical not well defined calculation which lead the pull variable to form a spike over that particular bin. The results of the 22^{nd} integration for the bin with values of $\Delta JES = 3\sigma$ and $M_t = 187.5 GeV/c^2$ are reported in table 2.2.

The fluctuation of only two results of integration over the minimum result not interpreted as 0 by the ME code force the mean over that event to be different from 0. Subsequently, the pull variable for all those zero results is fixed at that certain bin in

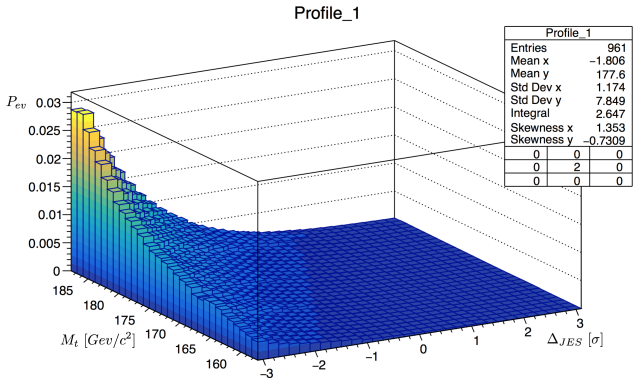

Figure 2.5: Plot of $W_{ij,ev=330}(\Delta_{JES}, M_t)$

the pull histogram. The same happens for the rest of the bins ij which show an analogous extremely low value the weight. In fact by looking at the pull distribution calculated only for event 330 (as shown in figure 2.6) we can clearly see how the distribution is extremely picked around $\sim$ 0.2. Those entries were creating the spike.

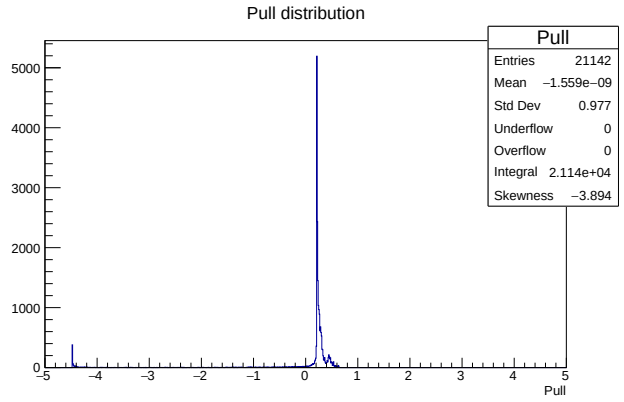

Figure 2.6: Pull histogram event 330 of q-MC integration method.

It is important to understand that for events with those kind of extreme kinematics the result of the integration was reliable but there is a numerical limit over which the results are interpreted as 0. For the purposes of the study of the integration it is not important if we take out one event of the MC sample since only the integration method was tested. The aim is to see the integration code behaviour in independent integrations. In the context of the data analysis it is different of course. From this results we learn that in the MC events as well as in the data , there can be events for which the weight returned by the code is exactly zero due to finite precision of the machine and ME code. Because

$P_{ev=330}\ bin[3\sigma, 187.5GeV/c^2]$																					
0	0	0	0	0	0	0	0	0	0	0	0	0	$5.4 \cdot 10^{-13}$	0	0	0	$9.2 \cdot 10^{-16}$	0	0	0	0

Table 2.2: Results of the 22 integration of the matrix element for event 330 in the sample in the bin with $\Delta_{JES} = 3\sigma$ and $M_t = 187.5GeV/c^2]$

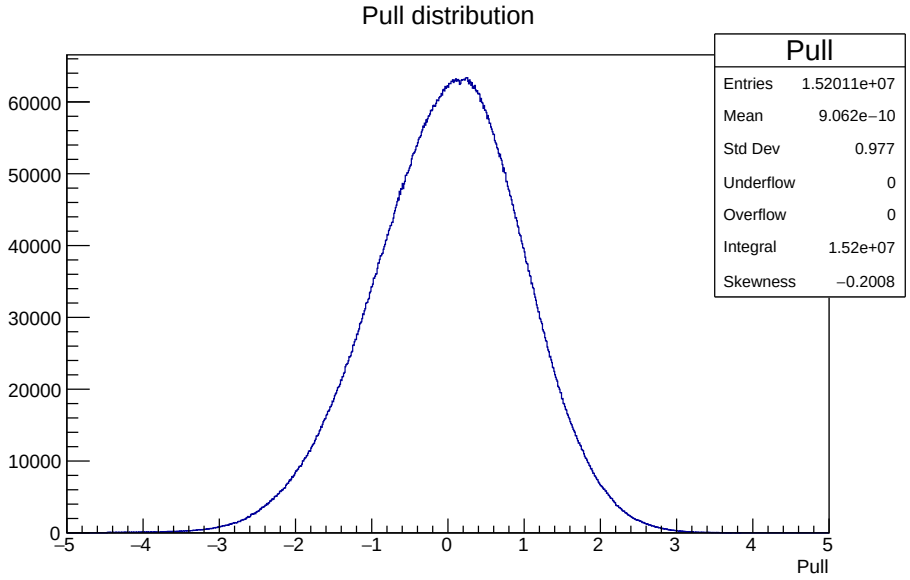

Figure 2.7: Pull histogram for q-MC integration meth without event 58 and 330 of the sample.

those weights, after normalisation, are probabilities with which we compute the likelihood (1.8), it is important to define how to deal with those events. One possibility is to put a cut on the likelihood in order to eliminate such events both in the testing with MC samples and on the analysis of the data. This will marginally reduce the size of the sample but will avoid such numerical problems. A similar cut on the likelihood was used in the last measurement [1].

Without those events the pull distribution is the one shown in figure 2.7.

$$\mu_{q-MC} = (9.0620 \pm 0.0003) \cdot 10^{-10}; \quad (2.14)$$

$$\sigma_{q-MC} = 0.9770 \pm 0.0001. \quad (2.15)$$

We see that it reproduce a gaussian distribution as expected meaning that the integration method using the scrambled sobol sequences is reliable. Still there is a negative skewness evident in the histogram. In this case also it is not clear if it will go away with more statistics (more repetition of every integration) or not. Anyway it is interesting to compare it to the pMC result. The pull distribution looks very similar. This ensure us that the q-MC integration method is as solid as it is the p-MC. Then if it reaches better convergence of the errors is undoubtedly a significant improvement over the code used in the last analysis. The fact that the two distribution looks so similar suggest that there could be a similar bias in the code independently of the sequence of point used. This also needs to be tested further.

2.3 Coefficient of variation: p-MC,q-MC

In order to have a qualitative results showing which is the more precise and better converging integration method a further analysis has been carried out. In figure 2.8 there is the histogram showing the ratio:

$$r_{k,ij} = \frac{\sigma_{k,ij}}{< W_{k,ij} >} \quad (2.16)$$

for the results of both the integration methods. This represents the coefficient of variation for every set of 22 repetitions of the various integrations.

We clearly see how this ratio is consistently smaller for q-MC method. The mean values of the histograms are:

$$\mu_{p-MC} = 0.11400 \pm 0.00008 \quad (2.17)$$

$$\mu_{q-MC} = 0.09363 \pm 0.00009 \quad (2.18)$$

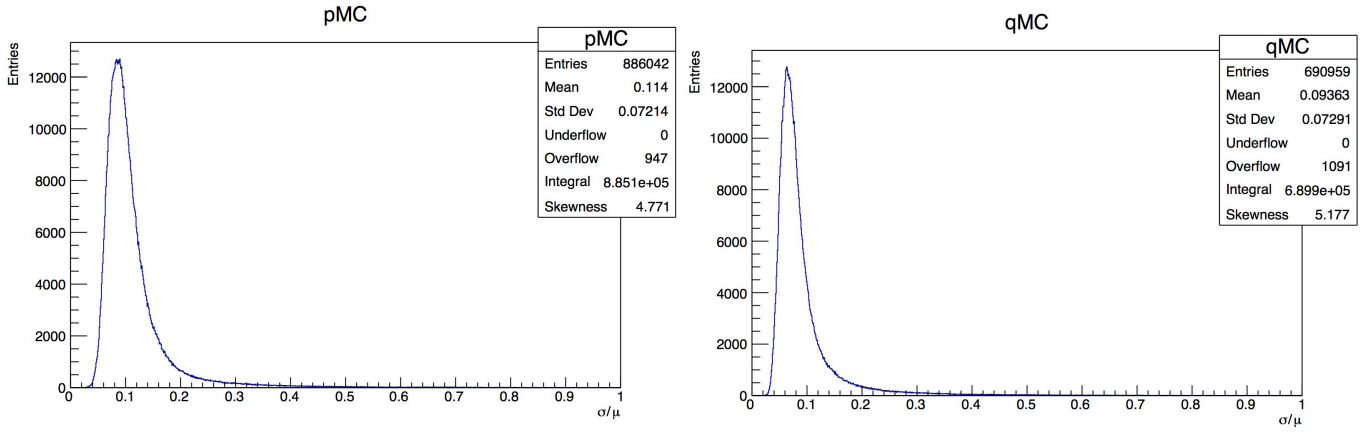

Figure 2.8: Histogram of the coefficient of variation for p-MC and q-MC

Since the two sets of simulation were run with the same termination parameters presented in section 2 and that, in this conditions, the integration is almost certainly stopped by reaching the integration time limit, the fact that we see a mean value of the ratio r smaller for q-MC than p-MC method is a qualitative proof that the latest integration method leads to a faster convergence and a more precise result overall. In order to have a quantitative estimation of the convergence the test needs to be repeated with the two method without termination parameters and fixed number of points. The speed of integration was preliminary tested with fixed number of points and it has been shown that there is no difference with the two methods.

Having a faster converging method finally leads to more precise results because in the refinement and calibration of the method (with pseudo-experiment) and finally in the data analysis the most constraining termination parameter is going to be the time limit. Thus, reaching a better precision with less points of integration will end up giving more precise results.

3 New Transfer Functions

The next part of analysis that I carried out is the comparison of the new and old transfer functions. The old TF have been used in the analysis up to this point and they are designed to be implemented in the ME code and used with only tight categories, see table 1.2. The new TF instead are compatible also with events in the loose categories. This is part of the improvement of the analysis with respect to the last CDF top mass measurement which didn't contain loose categories in the selected event sample.

In order to have a meaningful feedback to start debugging the new TF there are two possible ways: direct computation of same events in tight categories with both TF and comparison of the results; plot directly both TF to see what are the main differences. I compared them using the first method.

In the tight categories on which both are applicable (old TF were not derived to be used with loose categories) we should expect to get the same results. Therefore, I computed the likelihood for the 956 events from sample used in the pull analysis (A.1) with the old and new TF.

Approximatively $\sim 30\%$ of the events calculated with the new TF went on held status on Fermigrid because problems (Aborts, unphysical efficiencies...). Thus only the events that were successfully computed with the new TF where considered in both samples for the comparison. Of course the presence of such errors in the computation of the results for so many events give the first intuition that the new TF still need to be refined.

Firstly I computed the total likelihood as explained in section 1.3. As estimator for M_t and Δ_{JES} I extracted the values of the bin with maximum $log(L)$. It has to be underlined that the likelihood is still not the final likelihood because W_{ij} is still the unnormalised probability. In order to do the proper analysis we'll need to divide the weights by the acceptance and total cross section and extract the parameter with the profiled likelihood method. This has not been done in this section of the analysis since the aim of this work is to show a the qualitative difference in the results with different TF. They still present an important deviation from the origi-

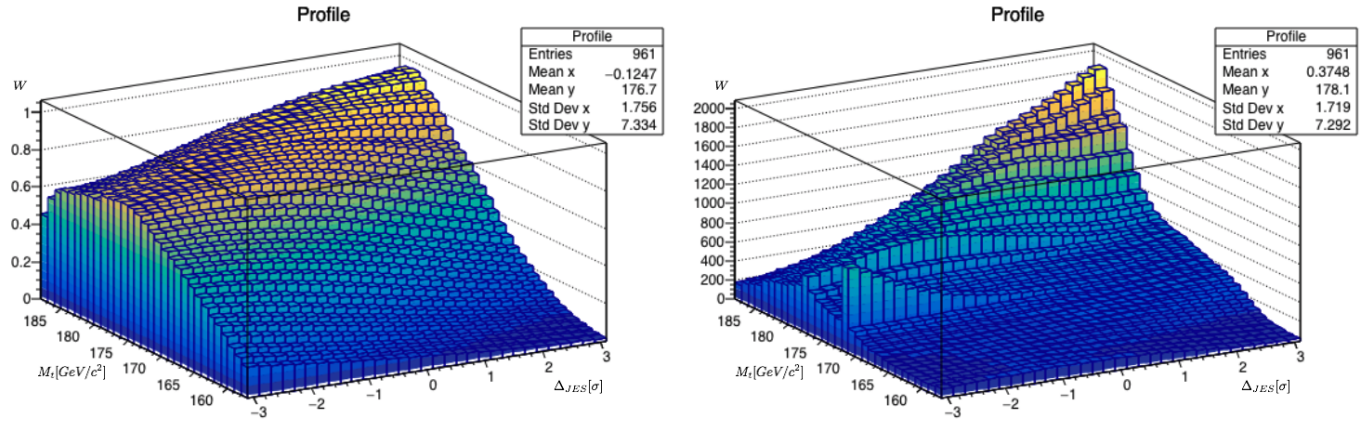

Figure 3.1: Comparison of single event from the sample computed with old/new TF

nal TF that quantitative results are not needed at this point. Results are shown in section 3.1 and 3.2.

In figure 3.1 we can see the result for a single event. On the left there is the result for the old TF while on the right for the new. It is evident how the new one present some bugs. For example we can spot the irregular behaviour of bin $171.5 GeV/c^2$ which is not expected. The other important thing to notice is that, even though the results are not normalised probabilities, the two plots show complete different order of magnitude for the weights resulting from the integration, meaning that there is a problem with the new TF normalisation.

3.1 Old transfer functions

MC Sample		Results	
$M_{t,MC}$	$173 GeV/c^2$	M_t	$172.5 GeV/c^2$
$\Delta_{JES,MC}$	0σ	Δ_{JES}	-1σ

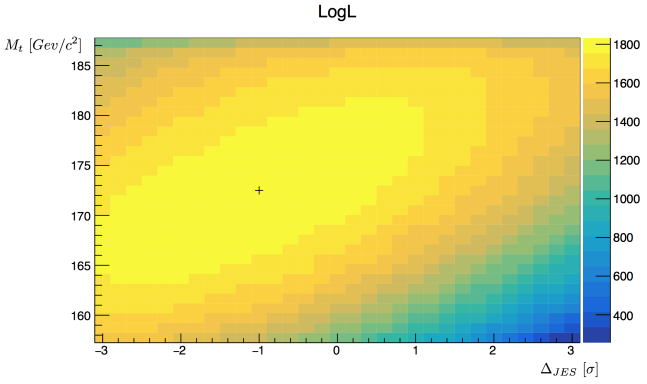

Figure 3.2: Old TF: contour plot of $Log(L)(\Delta_{JES}, M_t)$. The maximum bin is identified by a marker.

3.2 New Transfer Functions

MC Sample		Results	
$M_{t,MC}$	$170 GeV/c^2$	M_t	$178.5 GeV/c^2$
$\Delta_{JES,MC}$	0σ	Δ_{JES}	2σ

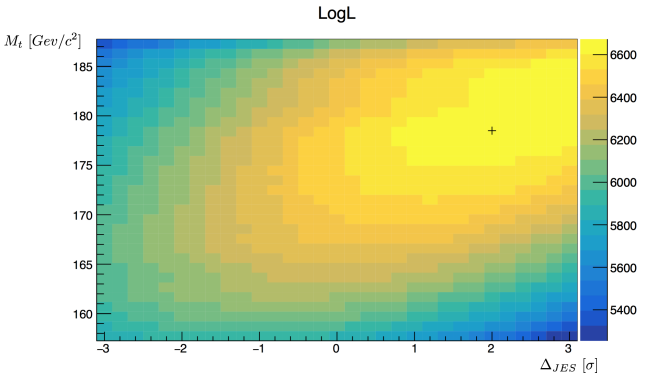

Figure 3.3: New TF: contour plot of $Log(L)(\Delta_{JES}, M_t)$. The maximum bin is identified by a marker.

3.3 Comparison of Results

The main conclusions we can draw from those results are the following. First of all the new TF gives weight which seems to be normalised differently compared to the old one so the normalisation has to be debugged (see image 3.1). Secondly, the new one gives unregular results which could be caused by a bug in the construction code. Lastly, by analysing the total likelihood over 700 events we can see clearly how the new one tend to underestimate the parton p_t which results in a shift of the max likelihood to the value of 2σ.

Since the new transfer functions where derived using NLO MC and with a different variables definition, possible errors could be present at various steps in their construction. This qualitative analysis was meant to identify possible problems by seeing the overall result in the likelihood.

4 Study of the sensitivity to Δ_{JES}

In this section I report the analysis I did on the sensitivity of the resulting estimators of M_t and Δ_{JES} to the shift of Δ_{JES} applied in the MC simulated signal events. This analysis is important at this stage of the measurement because, even though we do not have the complete likelihood definition, it checks if the the results for the parameters follows a linear dependence to the $\Delta_{JES,MC}$. If that is true, shifted results from the input MC values are going to be fixed with the final calibration of the method by means of pseudo-experiment.

The samples (A.1) used contain signal events generated at LO with Pythia with values of the $\Delta_{JES} = \{0, \pm 1\}\sigma$, $M_t = 172.5 GeV/c^2$, category 1TagT and 2TagT. The code used for the analysis is the signal matrix element code with the old transfer functions.

For every sample 10000 events were analysed in the following way. After having calculated the $2D$ likelihood, by using the profile likelihood method [11] the $1D$ likelihood over M_t and Δ_{JES} has been created. In general, to profile the $Log(L)(\Delta_{JES}, M_t)$ and extract the $Log(L)(M_t)$, the profile likelihood method impose to take for every bin in M_t the corresponding $Log(L)$ value defined as the maximum over all values of Δ_{JES} for that bin:

$$log(L)(M_t) = Max_{\forall i, j=M_t}\{log(L)ij\} \qquad (4.1)$$

The same procedure can be used to derived the profiled likelihood for the Δ_{JES} [2].

To extract the estimator and the 1σ uncertainty the histograms were fitted with a parabola. Then the estimator for M_t is the value that maximises the likelihood. The 1σ uncertainty is found by taking M_t^* so that:

$$log(L)(M_T^*) = log(L)_{Max} - 0.5. \qquad (4.2)$$

The profiled likelihood for M_t was fit in the range $M_t \in [160, 185] GeV/c^2$ to avoid the non parabolic behaviour of the tails of the histogram. Finally, I plotted the contour lines for the $2D$ likelihood which identify the 1σ, 2σ, 3σ uncertainty regions.

$$log(L)(\Delta_{JES}, M_T) = log(L)_{Max} - 0.5 \qquad (4.3)$$
$$log(L)(\Delta_{JES}, M_T) = log(L)_{Max} - 2 \qquad (4.4)$$
$$log(L)(\Delta_{JES}, M_T) = log(L)_{Max} - 4.5 \qquad (4.5)$$

This analysis follows the one explained in the article of the precedent measurement [5].

In the following sections 4.1, 4.3, 4.3 are reported the results for the three different samples.

4.1 $\Delta_{JES,MC} = -1\sigma$

In table 4.1 are reported the vales of the parameters which were used to generated the MC sample. Underneath there are the estimated M_t and Δ_{JES} from the fit of the profiled likelihood.

Sample = ttop25_mc_jes-1_btag_jpt20_.hs	
$M_{t,MC}$	$172.5 GeV/c^2$
$\Delta_{JES,MC}$	-1σ
Results	
$M_t(fit)$	$172.3 \pm 0.2\ GeV/c^2$
$\Delta_{JES}(fit)$	$-1.74 \pm 0.04\ \sigma$

Table 4.1: MC values and results

In appendix A.2 can be found the plot of the profiled likelihood and the corresponding fit. In figure 4.1 there is the contour plot of the $Log(L)$. After

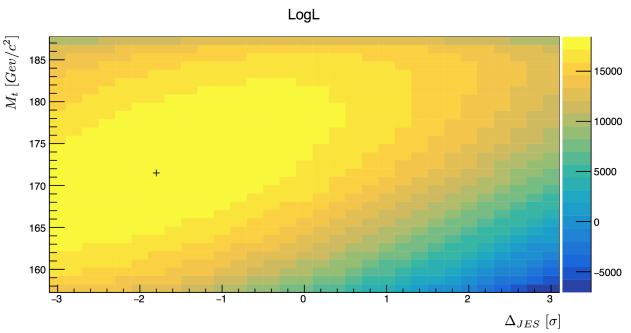

Figure 4.1: Contour plot of $log(L)$. The cross identify the bin with max value.

the 2D fit the contour plot was built (figure 4.2).

[2] In the limit of large statistics we expect the likelihood to follow a gaussian distribution. Since we have the unnormalised probabilities (missing total cross section and acceptance) to build the likelihood, this is of course an approximation. Since we expect the normalisation to be considerably flat over the parameter space, it doesn't change significantly the shape of the likelihood making this approximation less significant.

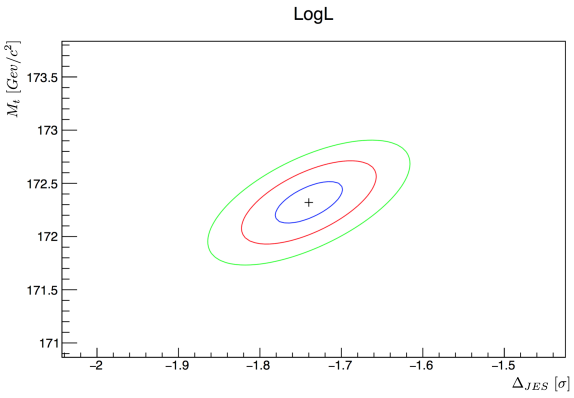

Figure 4.2: log(L) with contours corresponding to a 1-σ, 2-σ, and 3-σ uncertainty. The marker shows the maximum.

4.2 $\Delta_{JES,MC} = 0\sigma$

In table 4.2 are reported the vales of the parameters which were used to generated the MC sample. Underneath there are the estimated M_t and Δ_{JES} from the fit of the profiled likelihood.

Sample = ttop25_mc_jes0_btag_jpt20_.hs	
$M_{t,MC}$	$172.5 GeV/c^2$
$\Delta_{JES,MC}$	0σ
Results	
$M_t(fit)$	$170.9 \pm 0.2\ GeV/c^2$
$\Delta_{JES}(fit)$	$-1.32 \pm 0.05\ \sigma$

Table 4.2: MC values and results

In appendix A.3 can be found the plot of the profiled likelihood and the corresponding fit. In figure 4.3 there is the contour plot of the $Log(L)$.

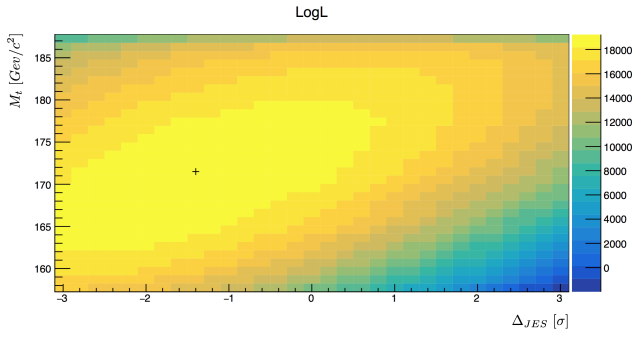

Figure 4.3: Contour plot of $log(L)$. The cross identify the bin with max value.

After the 2D fit the contour plot was built (figure 4.4).

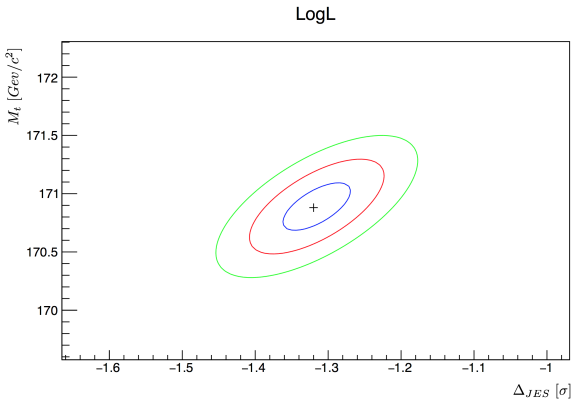

Figure 4.4: log(L) with contours corresponding to a 1-σ, 2-σ, and 3-σ uncertainty. The marker shows the maximum.

4.3 $\Delta_{JES,MC} = 1\sigma$

In table 4.3 are reported the vales of the parameters which were used to generated the MC sample. Underneath there are the estimated M_t and Δ_{JES} from the fit of the profiled likelihood.

Sample = ttop25_mc_jes-1_btag_jpt20_.hs	
$M_{t,MC}$	$172.5 GeV/c^2$
$\Delta_{JES,MC}$	-1σ
Results	
$M_t(fit)$	$169.8 \pm 0.2\ GeV/c^2$
$\Delta_{JES}(fit)$	$-0.90 \pm 0.05\ \sigma$

Table 4.3: MC values and results

In appendix A.4 can be found the plot of the profiled likelihood and the corresponding fit. In figure 4.3 there is the contour plot of the $Log(L)$.

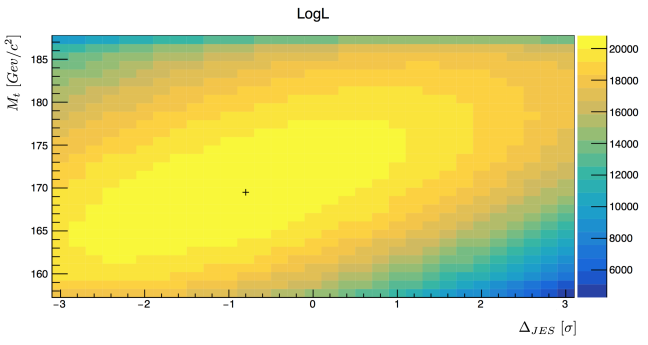

Figure 4.5: Contour plot of $log(L)$. The cross identify the bin with max value.

After the 2D fit the contour plot was built (figure 4.6).

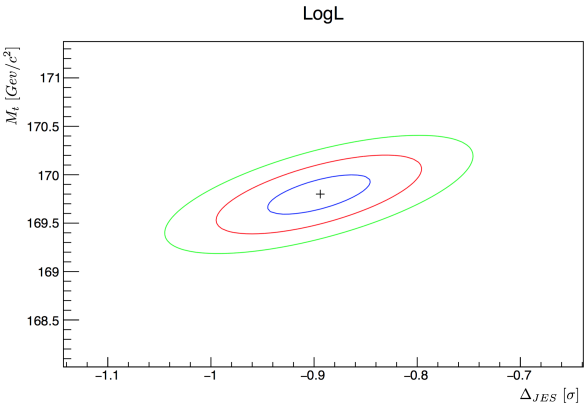

Figure 4.6: log(L) with contours corresponding to a 1-σ, 2-σ, and 3-σ uncertainty. The marker shows the maximum.

4.4 Results

In this subsection there is the summary of the results of this analysis. In table 4.4 we see the values of Δ_{JES} and M_t resulting from the analysis of each sample. Even though the results were derived with the unnormalised likelihood, at this stage of the analysis the goal was to see the dependencies to the shift of Δ_{JES} in the MC samples. We can see in figure 4.7 that there is a perfectly linear dependence between MC's Δ_{JES} and the resulting Δ_{JES}.

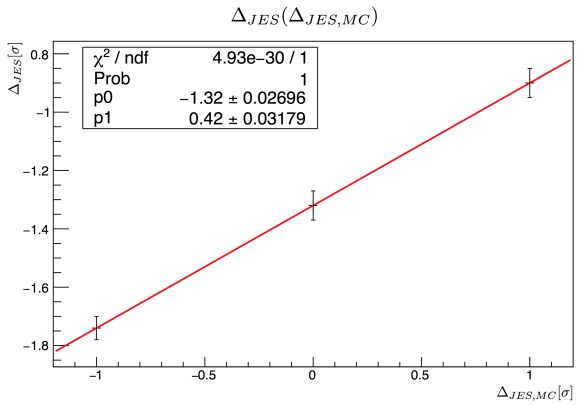

Figure 4.7: Plot of Δ_{JES} as a function of $\Delta_{JES,MC}$

$$\Delta_{JES} = [(-1.32 \pm 0.03) + (0.42 \pm 0.03) \cdot \Delta_{JES,MC}]\ \sigma \quad (4.6)$$

In fact a shift of absolute value 1 σ in MC's $\Delta_{JES,MC}$ creates a shift of 0.42σ in the Δ_{JES}. The linear dependence ensures that the shift absolute value and proportionality parameter will be corrected by the calibration that is going to be performed before the final measurement.

It is important to recall the definition of the Δ_{JES} used in by the CDF group for the construction of the sample. In an event generated with a certain Δ_{JES}, the actual correction applied to the jets is the opposite. For example, a sample with a positive Δ_{JES} has actually a negative correction to the $p_{t,jets}$ so that the likelihood itself will select a positive correction. For that reason we see a clear linear correlation.

Regarding the M_t linear dependence to the $\Delta_{JES,MC}$, we can see in figure 4.8 that there is an anti-correlation between MC's Δ_{JES} and M_t. This is the expected results following our definition of the JES correction in the construction of the sample: an overestimation of the jet energy scale ($\Delta_{JES} < 0$, as explained before) result in a greater value of the mass and vice-versa. A shift of absolute value 1 σ in MC's Δ_{JES} creates a shift of $\sim 1.25 GeV/c^2$ in the M_t.

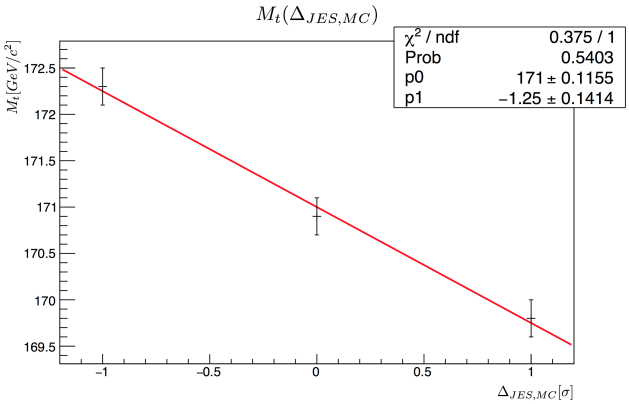

Figure 4.8: Plot of M_t as a function of $\Delta_{JES,MC}$

$$M_t = [(171.00 \pm 0.12) + (-1.25 \pm 0.14)\Delta_{JES,MC}]\ GeV/c^2 \quad (4.7)$$

Also in this case the linear dependence was expected and the values of the shifts after the inclusion of the proper normalisation are going to be tuned to the correct ones before the final measurement with the calibration performed with pseudo-experiments.

A note has to be added to this part of the analysis. The introduction of the normalisation with the acceptance (dependent on M_t and Δ_{JES}) and the total cross-section (dependent on M_t only) may change the location of the peaks in the log(L) but we don't expect that to change the linear dependence shown in this analysis.

Sample's Δ_{JES}	-1σ	0σ	1σ
$M_t(fit)$	$172.3 \pm 0.2\ GeV/c^2$	$170.9 \pm 0.2\ GeV/c^2$	$169.8 \pm 0.2\ GeV/c^2$
$\Delta_{JES}(fit)$	$-1.74 \pm 0.04\ \sigma$	$-1.32 \pm 0.05\ \sigma$	$-0.90 \pm 0.05\ \sigma$

Table 4.4: Results of the analysis of the three different samples

5 Conclusion

In this section I can summarise the current situation of the analysis with the insight given from the result of my work.

The q-MC integration code is giving reliable results and its improvements are going to be an important advantage in terms of precision of the results and machine time during the calibration and final measurement. There can be found the same slight deviation from gaussian behaviour in the pull with both the integration method which suggests that a bias could be present in the ME code itself. The next testing of the q-MC integration method should be done once a new definition of the integration errors is implemented in the code. The precise testing of the integral convergence will then be done to definitely validate the method

The main concern right now is the strange behaviour of the new transfer functions which is not well understood and needs to be fixed since they are the key element in the extension of the analysis with the inclusion of loose categories. They are going to be also a noticeable improvement compared to the last measurement since they are derived from Powheg NLO generated MC signal samples instead of LO Phytia MC signal samples.

The study of the sensitivity to the Δ_{JES} is also an important part in the validation of the signal code since it proved that the final calibration is going to fix perfectly the bias present in the analysis code. Furthermore, this analysis basically laid the footprint for the study of the systematic uncertainties resulting from the uncertainties in Δ_{JES}.

This report describe briefly the work I conducted at Fermilab under the supervision of Prof. Velev. The main results of the work I did during the summer school period are presented in section 2, 3, 4. Those results have been presented to the group conducting the measurement and has been posted on the internal webpage for future reference. Those are preliminary results since the analysis has still few steps to be performed before to approach the final measurement. Still, most of the macros developed by me are going to be useful for future analysis of the MC simulation and in the measurement itself. The aim of this measurement is to reduce the systematic and statistical uncertainties of the last measurement and reach the maximum precision with the complete RunII data sample.

I would like to thank my supervisor Prof. Velev for his advices and his patience. Furthermore, I would like to thank everyone involved in the analysis, in particular Prof.Vellidis which followed me as well and was very helpful; Tony which explained me quite a few mathematical subtleties and with which I had fruitful discussions. Prof. Volobuev for his professionalism and attention to our requests. Finally I would like to thank the organisers of the summer school, Prof. Bellettini, Dott. Barzi, Prof. Donati for having given me the opportunity to be part of the Fermilab summer school program.

References

[1] T. Aaltonen et al., *Top Quark Mass Measurement in the Lepton plus Jets Channel Using a Modified Matrix Element Method*, Phys. Rev. **D79** (2009), 072001.

[2] CMS D0 Collaborations ATLAS, CDF, *First combination of tevatron and lhc measurements of the top-quark mass*, (2014).

[3] CDF Collaboration and D0 Collaboration, *Tevatron combination of single-top-quark cross sections and determination of the magnitude of the cabibbo-kobayashi-maskawa matrix element V_{tb}*, Phys. Rev. Lett. **115** (2015), 152003.

[4] D0 Collaboration, *Precision measurement of the top quark mass in $lepton+jets$ final states*, Phys. Rev. Lett. **113** (2014), 032002.

[5] T. Aaltonen et al. (CDF Collaboration), *Top quark mass measurement in the lepton + jets channel using a matrix element method and in situ jet energy calibration*, Phys. Rev. Lett. **105** (2010), 252001.

[6] V. Khachatryan et al. (CMS Collaboration), *Measurement of the top quark mass using proton-proton data at* $\sqrt{(s)} = 7$ *and 8 tev*, Phys. Rev. D **93** (2016), 072004.

[7] Hee Sun Hong and Fred J. Hickernell, *Algorithm 823: Implementing scrambled digital sequences*, ACM Trans. Math. Softw. **29** (2003), no. 2, 95–109.

[8] R. Kleiss and W. J. Stirling, *Top quark production at hadron colliders: Some useful formulae*, Zeitschrift für Physik C Particles and Fields **40** (1988), no. 3, 419–423.

[9] H. Niederreiter, *Random number generation and quasi-monte carlo methods*, CBMS-NSF Regional Conference Series in Applied Mathematics, Society for Industrial and Applied Mathematics (SIAM, 3600 Market Street, Floor 6, Philadelphia, PA 19104), 1992.

[10] K. A. Olive et al., *Review of Particle Physics*, Chin. Phys. **C38** (2014), 090001.

[11] G.A. Young and R.L. Smith, *Essentials of statistical inference*, Cambridge Series in Statistical and Probabilistic Mathematics, Cambridge University Press, 2005.

A Appendices

A.1 Minintuples input files used in the analysis

- Pull distribution p-MC and q-MC:
  - ttbar_calib_djes0_notau_jpmatching_tight1tag_1000ev.ttkt73-htmtmu_mc.hs;
- Transfer functions comparison:
  - ttbar_calib_djes0_notau_jpmatching_tight1tag_1000ev.ttkt73-htmtmu_mc.hs;
- Analysis of the sensitivity to Δ_{JES}:
  - ttop25_mc_jes-1_btag_jpt20_.hs
  - ttop25_mc_jes0_btag_jpt20_.hs
  - ttop25_mc_jes1_btag_jpt20_.hs

A.2 $\Delta_{JES,MC} = -1\sigma$

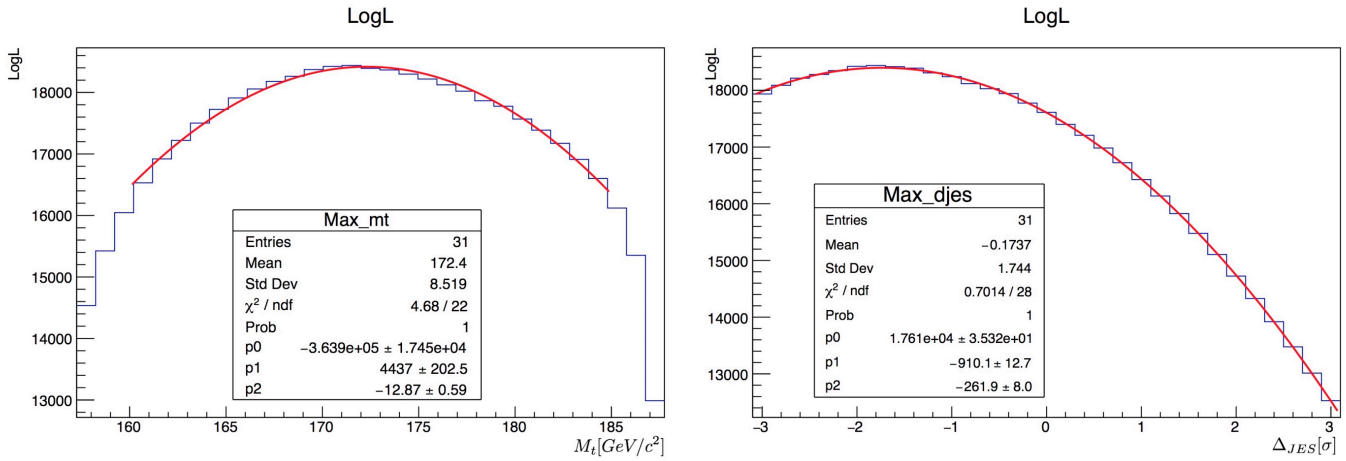

Figure A.1: Fit of the profiled Log(L) for both the parameter.

A.3 $\Delta_{JES,MC} = 0\sigma$

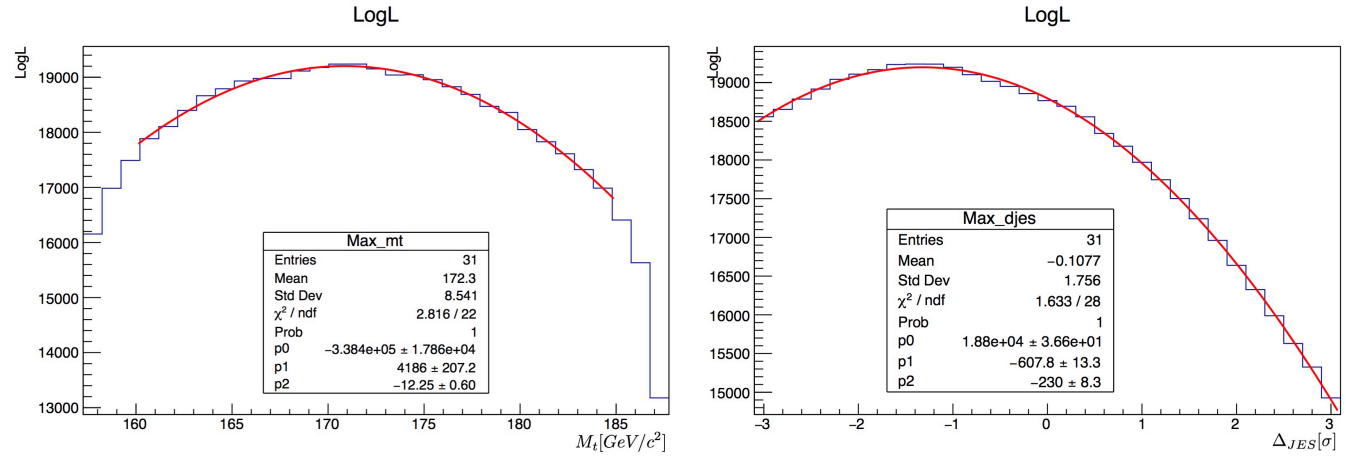

Figure A.2: Fit of the profiled Log(L) for both the parameter.

A.4 $\Delta_{JES,MC} = 1\sigma$

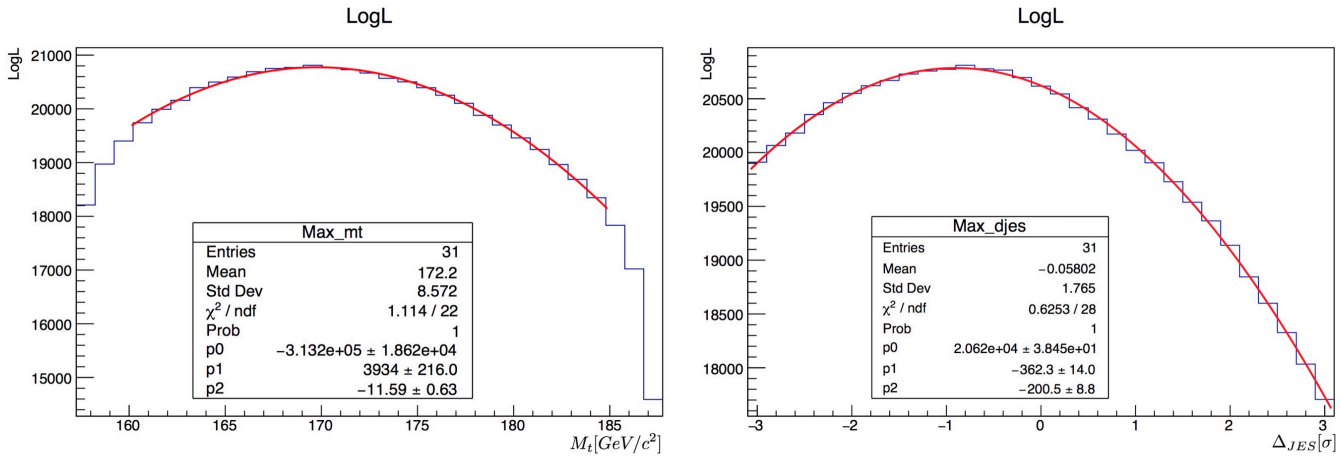

Figure A.3: Fit of the profiled Log(L) for both the parameter.